Effect of Serinate Ligation at Each of the Iron Sites of the [Fe_4S_4] Cluster of *Pyrococcus furiosus* Ferredoxin on the Redox, Spectroscopic, and Biological Properties†

Phillip S. Brereton, Randall E. Duderstadt, Christopher R. Staples, Michael K. Johnson, and Michael W. W. Adams*

Departments of Biochemistry & Molecular Biology and Chemistry and Center for Metalloenzyme Studies, University of Georgia, Athens, Georgia 30602

Received March 23, 1999; Revised Manuscript Received June 2, 1999

ABSTRACT: *Pyrococcus furiosus* ferredoxin (Fd) contains a single [Fe_4S_4] cluster coordinated by three cysteine (at positions 11, 17, and 56) and one aspartate ligand (at position 14). In this study, the spectroscopic, redox, and functional consequences of D14C, D14C/C11S, D14S, D14C/C17S, and D14C/C56S mutations have been investigated. The four serine variants each contain a potential cluster coordination sphere of one serine and three cysteine residues, with serine ligation at each of the four Fe sites of the [Fe_4S_4] cluster. All five variants were expressed in *Escherichia coli*, and each contained a $[Fe_4S_4]^{2+,+}$ cluster as shown by UV−visible absorption and resonance Raman studies of the oxidized protein and EPR and variable-temperature magnetic circular dichroism (VTMCD) studies of the as-prepared, dithionite-reduced protein. Changes in both the absorption and resonance Raman spectra are consistent with changing from complete cysteinyl cluster ligation in the D14C variant to three cysteines and one oxygenic ligand in each of the four serine variants. EPR and VTMCD studies show distinctive ground and excited state properties for the paramagnetic $[Fe_4S_4]^+$ centers in each of these variant proteins, with the D14C and D14C/C11S variants having homogeneous $S = {}^1/_2$ ground states and the D14S, D14C/C17S, and D14C/C56S variants having mixed-spin, $S = {}^1/_2$ and ${}^3/_2$ ground states. The midpoint potentials (pH 7.0, 23 °C) of the D14C/C11S and D14C/C17S variants were unchanged compared to that of the D14C variant ($E_m = -427$ mV) within experimental error, but the potentials of D14C/C56S and D14S variants were more negative by 49 and 78 mV, respectively. Since the VTMCD spectra indicate the presence of a valence-delocalized $Fe^{2.5+}Fe^{2.5+}$ pair in all five variants, the midpoint potentials are interpreted in terms of Cys11 and Cys17 ligating the nonreducible valence-delocalized pair in D14C. Only the D14S variant exhibited a pH-dependent redox potential over the range of 3.5−10, and this is attributed to protonation of the serinate ligand to the reduced cluster ($pK_a = 4.75$). All five variants had similar K_m and V_m values in a coupled assay in which Fd was reduced by pyruvate ferredoxin oxidoreductase (POR) and oxidized by ferredoxin NADP oxidoreductase (FNOR), both purified from *P. furiosus*. Hence, the mode of ligation at each Fe atom in the [Fe_4S_4] cluster appears to have little effect on the interaction and the electron transfer between Fd and FNOR.

Pyrococcus furiosus ferredoxin (Pf Fd)[1] is a low-molecular mass protein that contains a single [Fe_4S_4] cluster (*1*, *2*). It is typical of the cubane-type Fds with respect to its size (7500 Da), acidic charge at neutral pH, and its low reduction potential. However, it differs from most other Fds in two important aspects. First, it is remarkably thermostable, exhibiting limited degradation after several days at 95 °C. Second, it contains incomplete Cys ligation to the 4Fe cluster, as the second Cys in the conserved cluster binding motif C-X_2-C-X_2-C-X_3-C-P is replaced with an Asp residue in Pf Fd (Figure 1). While this is not unprecedented in Fds or in other Fe−S proteins, it is unusual, and in the case of Pf Fd allows for the quantitative removal of the Fe ligated by the Asp ligand (*2*). The cluster, at least in vitro, is readily interconverted between the $[Fe_4S_4]^{2+,+}$ and $[Fe_3S_4]^{+,0}$ forms, although this is not thought to have a physiological role.

† This work was supported by a grant from the NIH (GM45597 to M.W.W.A. and M.K.J.) and a NSF Research Training Group Award to the Center for Metalloenzyme Studies (DBI-9413236).

* To whom correspondence should be addressed: Department of Biochemistry, Life Sciences Building, University of Georgia, Athens, GA 30602-7229. Telephone: (706) 542-2060. Fax: (706) 542-0229. E-mail: adams@bmb.uga.edu.

[1] Abbreviations: aa, amino acids; Av, *Azotobacter vinelandii*; CAPS, 3-(cyclohexylamino)-1-propanesulfonic acid; CHES, 2-(*N*-cyclohexylamino)ethanesulfonic acid; Ca, *Clostridium acidi urici*; Cp, *Clostridium pasteurianum*; Da, *Desulfovibrio africanus*; Dg, *Desulfovibrio gigas*; DMSO, dimethyl sulfoxide; ENDOR, electron nuclear double resonance; EPPS, *N*-(2-hydoxyethyl)piperazine-*N*′-3-propanesulfonic acid; Fd, ferredoxin; FNOR, ferredoxin NADP oxidoreductase; HEPES, *N*-(2-hydroxyethyl)piperazine-*N*′-2-ethanesulfonic acid; HiPIP, high-potential iron protein; MES, 2-(*N*-morpholino)ethanesulfonic acid; NMR, nuclear magnetic resonance; Pa, *Peptostreptococcus asaccharolyticus*; PEG, poly(ethylene glycol); Pf, *Pyrococcus furiosus*; POR, pyruvate ferredoxin oxidoreductase; Tl, *Thermococcus litoralis*; VTMCD, variable-temperature magnetic circular dichroism; WT, wild-type.

10.1021/bi990671d CCC: $18.00
Published on Web 07/16/1999

```
                  10          20          30
Pf Fd   AWKVSVDQDT CIGDAICASL CPDVFEMNDE GKAQP
Dg Fd      PIEVNDD CMACEACVEI CPDVFEMNEE GD---
Tl Fd    MKVSVDKDA CIGCGVCASI CPDVFEMDDD GKAKA
Da Fd   ARKFYVDQDE CIACESCVEI APGAFAMDPE IE---
Ca Fd      AYVINEA CISCGACEPE CP-VNAIS-S GD---
Cp Fd      AYKIADS CVSCGACASE CP-VNAIS-Q GD---
Pa Fd      AYVINDS CIACGACKPE CP-VNCIQ-Q G----
                   I  II      III

                40          50          60
Pf Fd   KVEVI EDEEL-YNCAK EAMEACPVSA ITIEEA
Dg Fd   KAVVI NPDSD-LDCVE EAIDSCPAEA IRS
Tl Fd   LVAET DLE-----CAK EAAESCPTGA ITVE
Da Fd   KAYVK DVEGASQEEVE EAMDTCPVQC IHWEDE
Ca Fd   DRYVI DADTC-IDCGA CAGV-CPVDA PVQA
Cp Fd   SIFVI DADTC-IDCGN CANV-CPVGA PVQE
Pa Fd   SIYAI DADSC-IDCGS CASV-CPVGA PNPED
                                    IV
```

FIGURE 1: Sequence comparison of Pf Fd (66 aa) with Dg FdII (57 aa), Tl Fd (59 aa), Da FdI (64 aa), Ca Fd (55 aa), Cp Fd (55 aa), and Pa Fd (55 aa). Fully conserved positions are represented by bold letters. The amino acids involved in ligating the "N-terminal" cluster in each Fd are denoted by the Roman numerals below the position. The cluster is always bound by three ligands in one motif and by a distant Cys in the C-terminal end of the protein. The cluster ligand labeled II is Cys in each case, with the exception of Asp in Pf Fd. Sequences are from refs *44* and *50*−*55*.

Fe−S proteins have been shown to carry out a diverse range of processes (*3*−*5*). While electron transfer is still the primary function of most Fe−S clusters, there are now a number of examples where the cluster is acting in other capacities. For example, Fe−S clusters, in whole or in part, constitute the active sites of a variety of redox and nonredox enzymes. The best characterized example is the citric acid cycle enzyme, aconitase, which utilizes a redox-inactive Fe−S cluster to catalyze the citrate to isocitrate dehydration−rehydration isomerization reaction (*6*). In the absence of substrate, the enzyme has a 4Fe cluster which is ligated by three Cys residues and a hydroxyl group. The substrate binds at the unique Fe to yield a six-coordinate Fe site (*6*). Fe−S clusters can also function as sensors to regulate gene expression or enzymatic activity. For example, the ability to assemble an Fe−S cluster appears to be used as an Fe sensor in the iron-responsive protein (IRP) (*6*), and Fe−S clusters are used to sense oxygen in the fumarate and nitrate reductase regulatory (FNR) protein (*7*), superoxide in the SoxR protein (*8*, *9*), and possibly nitric oxide in mammalian ferrochelatase (*10*). In addition, there is evidence that Fe−S clusters may also be able to mediate coupled electron and proton transfer. For example, the binding of a serine side chain and a backbone amide nitrogen to Fe sites on oxidation of the nitrogenase P cluster suggests that this cluster may function in coupling proton and electron transfer to the active site cluster (*11*), although the ligated serine residue is apparently not responsible for the pH dependence of the cluster's midpoint potential (*12*). Histidine ligation to the [Fe_2S_2] cluster in the Rieske protein (*13*) and to the distal [Fe_4S_4] clusters in a NiFe hydrogenase (*14*) and some Fe hydrogenases (*15*) may also serve a similar purpose.

What has become apparent with the ever-increasing range of functions discovered for biological Fe−S clusters is that these new roles are often associated with incomplete cysteinyl ligation. Clearly, this activates the cluster and facilitates novel chemistry. Thus, for 4Fe Fds, which function only in electron transfer, the cluster is typically coordinated by four cysteine ligands. Currently Pf Fd, in which an aspartate replaces one of the coordinating cysteine residues, is the only well-characterized example of a 4Fe Fd with incomplete cysteinyl ligation of the [Fe_4S_4] cluster. The aspartate ligation may be involved in gating electron transfer by offering a switch mechanism between mono- and bidentate coordination of the Fe atom (*16*). Site-directed mutagenesis provides a means of probing the functional significance and spectroscopic consequences of noncysteinyl ligation to Fe−S clusters. The approach taken herein utilizes a small, single-cluster Fd (Pf Fd) as a model for understanding how the properties of a biological [Fe_4S_4] cluster are perturbed by systematically replacing each individual coordinating cysteine with a serine residue. As yet, there have been no reported attempts to generate a set of Fd mutants that have each of the four ligands to a [Fe_4S_4] cluster individually changed to a non-cysteine ligand. However, systematic studies involving Cys-to-Ser mutations of each coordinating cysteine residue have been reported for the $Fe(SCys)_4$ center in rubredoxin (*17*) and [Fe_2S_2] centers in fumarate reductase (*18*) and 2Fe Fds (*19*−*21*). Attempts to heterologously express genes that would encode [Fe_4S_4]-containing Fds with a noncysteinyl cluster ligand have typically resulted in either unstable proteins that could not be detected or isolated, proteins containing [Fe_3S_4] rather than [Fe_4S_4] clusters, or proteins in which a rearrangement had occurred to allow a nearby noncoordinating residue to replace the mutated residue (see ref *22* and references therein). Furthermore, Pf Fd has an advantage for systematic mutagenesis studies with a $[Fe_4S_4]^{2+,+}$ center, since it contains no other clusters to complicate spectroscopic characterization. Previous mutagenesis studies involving ligands to $[Fe_4S_4]^{2+,+}$ clusters have involved multicluster systems, such as PsaC, DMSO reductase, nitrate reductase, fumarate reductase, Da Fd III, and Av Fd I (*23*−*33*).

In addition to its small size, high stability, and single Fe−S cluster, Pf Fd is an excellent model system to study since it is central to many metabolic reactions within its host cell. Thus, this Fd serves as an electron acceptor in a variety of reactions in the peptide and carbohydrate fermentation pathways of Pf. It functions as an oxidant for pyruvate ferredoxin oxidoreductase (POR; *34*) and glyceraldehyde-3-phosphate oxidoreductase (GAPOR; *35*), and it is the electron acceptor for enzymes oxidizing various aldehydes, formaldehyde, indolepyruvate, 2-ketoglutarate, and 2-keto-isovalerate (*36*−*39*). Pf Fd has also been shown to donate electrons to ferredoxin NADP oxidoreductase (FNOR; *40*). Thus, there are a variety of oxidoreductases that have been purified from Pf which function in vivo in either the oxidizing or reducing direction, and these can be used to study physiologically relevant, interprotein electron transfer with Pf Fd.

In the study reported here, we focus on serine as the noncysteinyl ligand in Pf Fd. This was chosen because of its structural similarity to cysteine and the crystallographic or NMR evidence of serinate Fe ligation in several mutant Fe−S proteins (*17*, *20*, *41*). Moreover, we have previously prepared the D14S mutant of Pf Fd, and shown that the serine is a cluster ligand (*42*) and that the resulting protein has anomalous redox, spectroscopic, and biological properties (*43*). The overall goal of this work was to examine the redox and functional characteristics and the detailed spectroscopic properties (absorption, VTMCD, EPR, and resonance Ra-

man) of a series of analogous mutants in which the $[Fe_4S_4]$ cluster has the same coordination, namely, via three cysteine and one serine ligand, but to vary the position of the serine ligand within the protein. The three cysteine ligands that coordinate the $[Fe_4S_4]$ cluster in the native protein are at positions 11, 17, and 56 (*44*, *45*). Hence, the three double mutants, D14C/C11S, D14C/C17S, and D14C/C56S, were prepared, and their properties are compared with those of the fourth member of the series, D14S, as well as with those of the parent D14C Fd. In all cases, the spectroscopic results show that $[Fe_4S_4]^{2+,+}$ clusters are assembled and the effects of the location of the serine ligand on the properties of the $[Fe_4S_4]$ cluster have been determined.

MATERIALS AND METHODS

Materials. Restriction and modifying enzymes, oligonucleotides, and *Escherichia coli* strain JM105 were obtained from Stratagene (La Jolla, CA). IPTG was from Alexis (San Diego, CA). Sequenase (version 2.0), casein hydrolysate, yeast extract, and ampicillin were purchased from U.S. Biochemical (Cleveland, OH). The radioactive nucleotide used for DNA sequencing was [α-^{35}S]dATP which was obtained from Amersham Corp. (Arlington Heights, IL). The expression plasmid pTrc99A and the chromatography materials (Sephadex G-75, Q-Sepharose Fast Flow, and Mono-Q) were from Pharmacia-LKB (Piscataway, NJ). The Mutagene kit was purchased from Bio-Rad (Richmond, CA). The antibiotic neomycin sulfate, buffers (CAPS, CHES, MES, HEPES, and EPPS), NADP, pyruvate, benzyl viologen, and methyl viologen were all from Sigma (St. Louis, MO). Coenzyme A was purchased from ICN (Costa Mesa, CA). The YM-3 ultrafiltration membranes were from Amicon (Beverly, MA). Al_2O_3 slurry and diamond polish were obtained from Buehler (Lake Bluff, IL). Tris-tricine gels were from Novex (San Diego, CA).

Mutagenesis and Expression. The cloning, mutagenesis, and expression of the various forms of Pf Fd mutants have been described previously (*43*, *45*, *46*). The double mutants described in this work (D14C/C11S, D14C/C17S, and D14C/C56S) were constructed by the method of Kunkel (*47*) using as a template the gene encoding the D14C variant that had already been through one cycle of PCR mutagenesis (*48*). The oligonucleotides used to introduce the mutations were 5′-ACA TCC TAT AGA GGT GTC TTG-3′ (C11S), 5′-GAG GCT TGC AGA GAT GGC ACA-3′ (C17S), and 5′-ACT AAC TGG AGA GGC CTC CAT-3′ (C56S). Expression conditions were identical to those described elsewhere (*43*). In brief, the mutant genes were cloned into the *Nco*I and *Pst*I sites of the vector pTrc99A. The plasmid was transformed into the expression strain *E. coli* JM105. The medium used was LB containing glycerol (0.5%). Induction with IPTG (1 mM) was achieved when the OD_{600} reached approximately 0.6 and cellular yields were 7−8 g (wet weight)/L.

Purification. Because of the possible O_2 sensitivity of the proteins containing a potential serine ligand to the Fe−S cluster of Pf Fd, all purification procedures were performed under anaerobic conditions with all buffers containing sodium dithionite (2 mM). *E. coli* cells (700−800 g) were lysed using lysozyme, and the lysed cells were incubated at 70 °C for 1 h and then stored at 4 °C overnight to denature *E. coli* proteins. Cellular debris and denatured protein were removed by centrifugation (11000*g* for 45 min; Beckman JA-10 rotor). The supernatant was diluted 3-fold with 50 mM Tris-HCl at pH 8.0 (buffer A) and loaded onto a Q-Sepharose Fast Flow column (7 cm × 23 cm) equilibrated with buffer A. The column was washed with buffer A (2 L), and the absorbed proteins were eluted with a linear gradient (5 L) from 0 to 0.6 M NaCl in buffer A. Fd (as judged by its brown color) was collected and concentrated by ultrafiltration (Amicon membrane), and applied to a column (6 cm × 60 cm) of Sephadex G-75, equilibrated with sodium phosphate (50 mM, pH 7.7) containing 5 mM dithionite, at a rate of 3 mL/min. Fractions containing pure Fd as judged by electrophoretic analysis on a native Tris-tricine polyacrylamide gel (16% w/v; *31*) and by the maximum value of the absorbance ratio (A_{390}/A_{280}) were combined and concentrated prior to storage under Ar at −80 °C. Native Tris-tricine polyacrylamide gels provide a convenient way of distinguishing between holo-Fd and apo-Fd. Under native, nondenaturing conditions, the two forms run very differently; the native folded form runs with the dye front, while the apo or unfolded form migrates significantly slower and more diffusely. Approximately 30 μg of Fd was loaded into each lane due to the poor staining of Fd with the Coomassie dye.

This purification scheme was sufficient to purify all mutant forms of the protein except for the D14C/C56S protein. Electrophoretic analysis (see below) showed there to be significant amounts of the apo form still present, and this was also manifested in a low absorbance ratio (A_{390}/A_{280}) for this protein. The D14C/C56S protein (approximately 6 mg/mL) was loaded (in 1 mL aliquots) onto a Mono-Q column (1 mL bed volume) equilibrated in buffer A containing NaCl (0.1 M). The protein was eluted with a linear gradient from 0.1 to 0.45 M NaCl in buffer A (30 mL). The D14C/C56S mutant eluted as 0.23−0.32 M NaCl was applied to the top of the column. The Fd fractions were collected, concentrated by ultrafiltration, and loaded onto a Sephadex G-75 column (2.6 cm × 60 cm), equilibrated with sodium phosphate (50 mM, pH 7.7) containing 5 mM dithionite, at a rate of 0.5 mL/min. Electrophoretic analysis showed the protein to be virtually homogeneous with a very small amount of remaining apoprotein. The A_{390}/A_{280} was significantly increased by this procedure (see the Results). The protein was concentrated and stored as described above.

Spectroscopic Methods. UV−visible absorption spectra of the oxidized and reduced forms of each mutant [at approximately 30 μM in 50 mM EPPS (pH 8.0)] were recorded on a Shimadzu UV-2501PC spectrophotometer at 23 °C. VTMCD spectra were collected on samples containing 55% (v/v) poly(ethylene glycol) (PEG) using a Jasco J715 spectropolarimeter mated to an Oxford Instruments Spectromag 4000 (0−7 T) split-coil superconducting magnet. The MCD intensities are expressed as $\Delta\epsilon$ ($\epsilon_{LCP} - \epsilon_{RCP}$) where ϵ_{LCP} and ϵ_{RCP} are the molar extinction coefficients for the absorption of left and right circularly polarized light, respectively, and the magnetic fields are given in the figure legends. X-band (~9.5 GHz) EPR spectra were obtained using a Brüker ESP-300E EPR spectrometer equipped with a dual-mode ER-4116 cavity and an Oxford Instruments ESR-9 flow cryostat. Frequencies were measured with either a Systron-Donner 6054B frequency counter or a Hewlett-Packard 5350B microwave frequency counter, and the

magnetic field was calibrated with a Bruker ER035M gaussmeter. Spin quantitations were carried out under nonsaturating conditions using 1 mM Cu(II)EDTA as the standard.

Resonance Raman spectra were recorded with an Instruments SA U1000 spectrometer fitted with a cooled RCA 31034 photomultiplier tube, using lines from a Coherent Innova 100 10 W Ar^+ laser or a Coherent Innova 200-K2 Kr^+ laser. Scattering was collected at 90° from the surface of a frozen 10 μL droplet of protein solution using an Air Products Displex model CSA-202E closed cycle refrigerator. Band positions were calibrated using the excitation wavelength, and are accurate to ± 0.5 cm^{-1}. Raman spectra of the same sample obtained at different wavelengths were normalized to the intensity of the ice band at 230 cm^{-1}, which serves as an internal standard. The spectrum of the frozen buffer solution, normalized to the intensity of the ice band at 231 cm^{-1}, and a linear ramp fluorescent background have been subtracted from all spectra described in this work.

Biological Assay. The biological activity of the Fd mutants was assessed in a coupled assay system in which Fd reduced by an excess of POR was subsequently oxidized by FNOR (*40*). It has been shown previously (*43*) that the reduction of the Fd variants, even those with redox potentials considerably lower than that of the wild-type protein, occurs much faster than the oxidation with FNOR in this assay system. The measured activity therefore reflects the Fd and FNOR association and electron-transfer step of the reaction. The assay (2 mL) was performed at 80 °C in EPPS buffer (50 mM, pH 8.0) containing pyruvate (10 mM), coenzyme A (0.2 mM), $MgCl_2$ (1 mM), Pf POR (20 μg/mL, 10 units/mg), and Fd (0.025−20 μM). The reaction was started by the addition of FNOR (5 μg/mL, 55 units/mg). The reaction was followed by measuring the reduction of NADP at 365 nm. A molar absorbance of 3400 M^{-1} cm^{-1} was used for NADPH. One unit of activity in this assay is 1 μmol of pyruvate oxidized per minute (equivalent to 2 μmol of Fd oxidized per minute). Curves were fitted with the Michaelis−Menten equation. The activity of FNOR was determined using the artificial electron acceptor benzyl viologen (1 mM) with NADH (0.3 mM) as the electron donor. One unit of activity of FNOR catalyzed the reduction of 2 μmol of benzyl viologen per minute in CAPS buffer (50 mM, pH 10.3). The activity of POR was determined independently under the same conditions but with methyl viologen (1 mM) replacing Fd as the electron acceptor. One unit of POR activity was defined as the oxidation of 1 μmol of pyruvate per minute.

Electrochemistry. The reduction potentials of the proteins and their pH dependence were measured by cyclic voltammetry at a glassy carbon electrode. The electrochemistry cell that was used was identical to that described by Hagen (*49*). The working electrode was prepared by polishing it with an Al_2O_3 slurry (0.3 μm) and then with diamond spray (1 μm). This was repeated for each measurement. The Fd double mutants (50−100 μM) in the appropriate buffer (50 mM citrate, formate, acetate, MES, HEPES, CHES, or CAPS) containing the promoter neomycin (2 mM) were analyzed between pH 3.5 and 10.0 at 23 °C. The scan rate was 10 mV/s over the potential range of −200 to −900 mV (vs the Ag/AgCl electrode). The working, counter, and reference electrodes were glassy carbon, Pt, and Ag/AgCl, respectively.

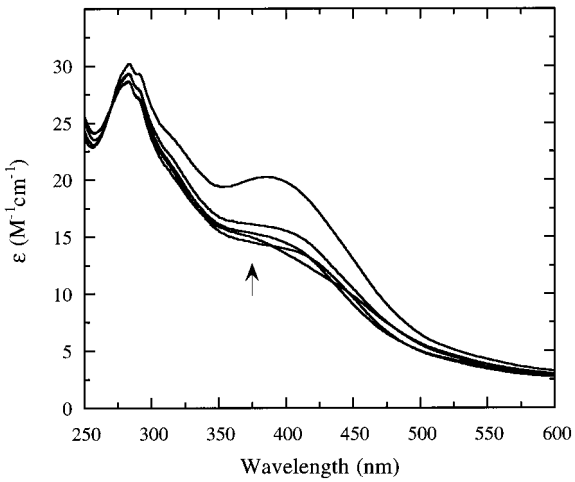

FIGURE 2: UV−visible spectra of air-oxidized variants of Pf Fd. The variants are, from top to bottom at 370 nm (denoted by the arrow), D14C, D14S, D14C/C17S, D14C/C56S, and D14C/C11S. The samples (approximately 30 μM) were in 50 mM EPPS buffer (pH 8.0), and the spectra were recorded at 23 °C.

RESULTS

Expression and Purification. As with the D14S and D14C variants of Pf Fd (*45*), the recombinant versions of the three double mutants, D14C/C11S, D14C/C17S, and D14C/C56S, expressed in *E. coli* all contained an Fe−S cluster, and the associated brown color facilitated their purification. However, the yield of each of the mutants was lower than those of the recombinant wild type, and the D14C and D14S variants, all of which are produced in comparable quantities. The D14C/C11S and D14C/C17S mutants were produced in amounts that were about 4−5 times lower than that of the wild-type protein, with yields of approximately 0.15 mg/g (wet weight) of *E. coli* cell paste. The D14C/C56S protein was isolated at significantly lower levels, approximately 0.01 mg/g (wet weight) of cells. However, each protein appeared to be stable, with no visible deterioration after 1 h at 70 °C or after several days at 25 °C under either aerobic or anaerobic conditions. Moreover, electrophoretic analyses of cell-free extracts (after the initial anion exchange step) did not identify any significant levels of apoprotein. Thus, the lower yields of the three Ser double mutants do not appear to be the result of degradation of the protein during purification but do appear to be the result of the lower amounts of holoprotein produced by *E. coli*. This is consistent with the general observation that in essence only holoproteins are produced in vivo because the (apo)polypeptides are susceptible to rapid degradation (*22*). In any event, all four Ser variants, with Ser at position 11, 14, 17, or 56, and with three Cys residues completing the likely cluster coordination sphere, were produced in a pure form.

UV−Visible Spectroscopy. The UV−visible absorption spectra of air-oxidized forms of D14C, D14C/C11S, D14S, D14C/C17S, and D14C/C56S Pf Fd are shown in Figure 2. The additional cysteinyl-S-to-Fe(III) charge-transfer intensity in D14C leads to a pronounced shoulder at 390 nm (*45*) and a concomitant increase in the absorbance ratio ($A_{390}/A_{280} = 0.73$) and extinction coefficient ($\epsilon_{390} = 20.2$ M^{-1} cm^{-1}) compared to those of the four serine mutants. As previously noted for the D14S variant (*45*), none of the Ser double mutants had a well-resolved band in the visible region.

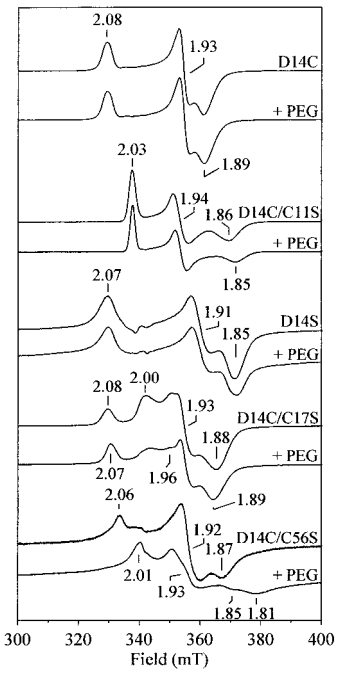

FIGURE 3: Perpendicular-mode X-band EPR spectra of $[Fe_4S_4]^+$ centers in dithionite-reduced D14C, D14C/C11S, D14S, D14C/C17S, and D14C/C56S Pf Fd in the $S = {}^1/_2$ region: 0.59 mM D14C, 0.85 mM D14C/C11S, 0.88 mM D14S, 1.02 mM D14C/C17S, and 0.72 mM D14C/C56S. All samples were in 100 mM Tris-HCl buffer (pH 7.8) except D14S which was in 100 mM CAPS buffer (pH 10.5), and samples were reduced by anaerobic addition of sodium dithionite to a final concentration of 2 mM. Conditions of measurement were as follows: microwave power, 1 mW; temperature, 10 K; microwave frequency, 9.61 GHz; and modulation amplitude, 0.64 mT. In each case, EPR spectra are also shown after the anaerobic addition of 55% (v/v) PEG, and the resulting D14C, D14C/C11S, D14S, D14C/C17S, and D14C/C56S samples were at concentrations of 0.27, 0.55, 0.40, 0.66, and 0.46 mM, respectively. The conditions of measurement were the same as those without PEG added.

Moreover, the absorption ratios and molar extinction coefficients of all four serine mutants are comparable; $A_{390}/A_{280} = 0.50$, 0.55, 0.51, and 0.50 and $\epsilon_{390} = 15.8$, 14.1, 14.9, and 14.2 M^{-1} cm^{-1} for D14C/C11S, D14S, D14C/C17S, and D14C/C56S, respectively. The spectra of each of the four Ser variants are comparable, although not identical, and consistent with the presence of a single $[Fe_4S_4]^{2+}$ cluster. However, due to the similarity in the absorption characteristics of $[Fe_4S_4]^{2+}$ and $[Fe_3S_4]^+$ clusters, in particular, this interpretation requires confirmation with spectroscopic techniques that are more discriminating with respect to cluster type.

EPR Spectroscopy. The absence of significant amounts of $S = {}^1/_2$ $[Fe_3S_4]^+$ clusters in air-oxidized samples of D14C, D14C/C11S, D14S, D14C/C17S, and D14C/C56S Pf Fd was demonstrated by EPR studies. All five variants exhibited negligible resonances in the $S = {}^1/_2$ region, accounting for <0.05 spin per molecule. X-band EPR spectra in the $S = {}^1/_2$ region of dithionite-reduced D14C, D14C/C11S, D14S, D14C/C17S, and D14C/C56S Pf Fd in the presence and absence of 55% (v/v) PEG are shown in Figure 3. As for $S = {}^1/_2$ $[Fe_4S_4]^+$ centers in other bacterial Fds, the resonances are fast-relaxing and only observable at temperatures below 30 K. The dithionite-reduced D14C/C11S mutant exhibits a rhombic EPR signal with g-values of 2.03, 1.94, and 1.86 ($g_{av} = 1.94$), accounting for 1.00 ± 0.05 spins per molecule at pH 7.8, indicative of a homogeneous $S = {}^1/_2$ $[Fe_4S_4]^+$ cluster. The g-value anisotropy is smaller than that of the aspartyl-ligated $S = {}^1/_2$ $[Fe_4S_4]^+$ cluster in the wild type ($g = 2.10$, 1.87, and 1.79; $g_{av} = 1.92$) (*2*) and comparable to that of the all-cysteinyl-ligated pure $S = {}^1/_2$ $[Fe_4S_4]^+$ cluster in D14C ($g = 2.08$, 1.93, and 1.89; $g_{av} = 1.97$). However, the g_{av}-value for the D14C/C11S variant is substantially reduced compared to that of the D14C variant. The dithionite-reduced D14S variant displays an $S = {}^1/_2$ EPR signal ($g = 2.07$, 1.91, and 1.85; $g_{av} = 1.94$) with greater anisotropy and faster relaxation compared to those of the other three Ser variants, but both the anisotropy and relaxation properties are intermediate between those of the $[Fe_4S_4]^+$ centers in the wild type and the all-cysteinyl-ligated D14C variant. The signal is only observable below 20 K, and spin quantitations of the $S = {}^1/_2$ resonance yielded values of 0.35 ± 0.05 spin per molecule at pH 7.8 and 0.60 ± 0.05 spin per molecule at pH 10.5. This is in accord with the midpoint potential (see below) and UV−visible absorption studies which show that the cluster is only partially reduced by dithionite at pH 7.8, but fully reduced at pH 10.5. The dithionite-reduced D14C/C17S variant exhibits a complex EPR signal in the $S = {}^1/_2$ region with inflections at g values of 2.08, 2.00, 1.93, and 1.88. This signal is only observable below 30 K and clearly consists of at least two distinct $S = {}^1/_2$ species. Attempts to differentiate the component species using power saturation at various temperatures ware unsuccessful. However, the addition of PEG perturbs the mixture and indicates that the $g = 2.00$ feature is the low-field component of a resonance that overlaps with a rhombic resonance ($g = 2.08$, 1.93, and 1.88; $g_{av} = 1.96$), which has g-values very similar to those of the $[Fe_4S_4]^+$ cluster in the all-cysteinyl-ligated D14C variant. The latter resonance dominates in the presence of PEG. Spin quantitations of this heterogeneous resonance yielded a value of 0.70 ± 0.05 spin per molecule at pH 7.8, in both the presence and absence of 55% (v/v) PEG. The dithionite-reduced D14C/C56S variant has an EPR signal ($g = 2.06$, 1.92, and 1.87; $g_{av} = 1.95$) with anisotropy and line widths most similar to those of the D14C/C17S and D14C variants. The signal is only observable below 25 K, and spin quantitations of the $S = {}^1/_2$ resonance gave values of 0.60 ± 0.07 spin per molecule at pH 7.8 and 0.75 ± 0.08 spin per molecule at pH 10.5, suggesting incomplete reduction by dithionite at pH 7.8. However, the addition of 55% (v/v) PEG causes a dramatic perturbation of the resonance, yielding a heterogeneous, fast-relaxing signal with the major component at $g = 2.01$, 1.93, and 1.81 ($g_{av} = 1.92$) more similar to that of the D14C/C11S variant.

The $[Fe_4S_4]^+$ cluster in reduced wild-type Pf Fd exists as an 80:20 mixture of $S = {}^3/_2$:$S = {}^1/_2$ ground states in frozen solution. Figure 4 compares the $S = {}^1/_2$ and $S = {}^3/_2$ regions of the EPR spectra of dithionite-reduced D14C/C11S, D14S, D14C/C17S, and D14C/C56S variants of Pf Fd. The $S = {}^1/_2$ regions for all spectra were recorded at 10 K, while the $S = {}^3/_2$ insets for D14S, D14C/C17S, and D14C/C56S were recorded at 4.2 K. In accord with the substoichiometric $S = {}^1/_2$ spin quantitations, the D14S, D14C/C17S, and D14C/C56S variants all exhibit $S = {}^3/_2$ resonances and hence are mixed-spin species. In contrast, the D14C/C11S and C14C variants have pure $S = {}^1/_2$ $[Fe_4S_4]^+$ clusters. The $S = {}^3/_2$ region of the D14S spectrum as prepared (in the absence of PEG) is dominated by a sharp feature at $g = 5.69$, a broad

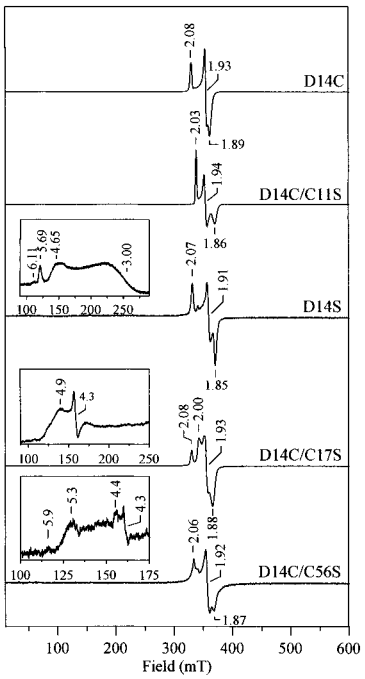

FIGURE 4: Perpendicular-mode X-band EPR spectra of $[Fe_4S_4]^+$ centers in dithionite-reduced D14C, D14C/C11S, D14S, D14C/C17S, and D14C/C56S Pf Fd $[Fe_4S_4]^+$ mutants in the $S = {}^1/_2$ and $S = {}^3/_2$ regions. The samples are the same as those used in the experiments whose results are depicted in Figure 3 and do not contain PEG. Conditions of measurement were the same as those described in the legend of Figure 3 for the $S = {}^1/_2$ region. For the $S = {}^3/_2$ regions (insets), the spectra were recorded at 4.2 K with a microwave power of 50 mW.

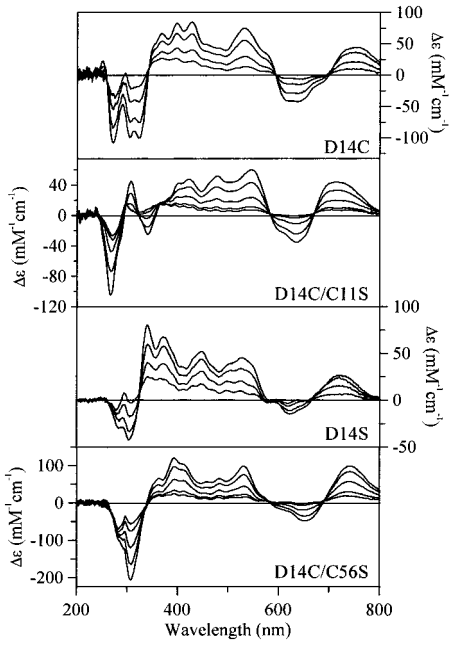

FIGURE 5: UV−visible VTMCD spectra of $[Fe_4S_4]^+$ centers in dithionite-reduced D14C, D14C/C11S, D14S, and D14C/C56S Pf Fd. All samples contain 55% (v/v) PEG and are in 100 mM Tris-HCl buffer (pH 8.0). D14C, at 0.36 mM, with MCD at 6.0 T and 1.63, 4.22, 9.7, 23, and 41 K. D14C/C11S, at 0.55 mM, with MCD at 6.0 T and 1.66, 4.22, 9.6, 23, and 41 K. D14S, at 0.28 mM, with MCD at 4.5 T and 1.61, 4.22, 10.3, and 25 K. D14C/C56S, at 0.46 mM, with MCD at 6.0 T and 1.78, 4.22, 9.7, 23, and 41 K. In all spectra, the MCD intensity at all wavelengths increases with decreasing temperature.

feature centered at $g = 4.65$, and a derivative-shaped feature centered at approximately $g = 3.0$. The relative intensities of the $g = 5.69$ and $g = 4.65$ resonances are invariant with increasing temperature; thus, they do not originate from different zero-field doublets within the same $S = {}^3/_2$ ground state manifold. This result indicates the presence of two distinct $S = {}^3/_2$ systems. One is a rhombic $S = {}^3/_2$ species, and a conventional spin Hamiltonian with an E/D of 0.33, and g_o predicts effective g-values of 5.6, 2.0, and 1.5 for both doublets. The second species is a more axial $S = {}^3/_2$ species with an E/D of 0.13 and a g_o of 2.0, predicting g-values of 5.90, 0.81, and 0.71 for the "$M_s = \pm{}^3/_2$ doublet" and g-values of 4.71, 3.19, and 1.90 for the "$M_s = \pm{}^1/_2$ doublet". Interestingly, the addition of 55% (v/v) PEG causes these two $S = {}^3/_2$ systems to collapse into a single homogeneous $S = {}^3/_2$ species in which the feature at $g = 4.65$ disappears and what remains is the feature at 5.69 and a very broad derivative that underlies the majority of the spectral range, and is centered between $g = 2.5$ and $g = 1.9$ (data not shown). The D14C/C17S sample also contains an $S = {}^3/_2$ component as evidenced by the broad resonance centered at $g = 4.9$. The derivative at $g = 4.33$ is attributed to adventitious high-spin Fe(III) ion. The $g = 4.9$ feature is indicative of an $S = {}^3/_2$ species with intermediate rhombicity ($E/D \sim 0.17$). Temperature dependence studies did not reveal any other well-resolved components, and the resonance is too weak to warrant more detailed analysis. Likewise, the D14C/C56S sample contains an $S = {}^3/_2$ component as evidenced by the pronounced resonance at $g = 5.3$. This is indicative of a more rhombic $S = {}^3/_2$ species ($E/D \sim 0.27$). Temperature dependence studies suggested heterogeneity in the $S = {}^3/_2$ species, with the $g = 5.9$ and 4.4 features originating from a more axial ($E/D \sim 0.07$) species. However, the weakness of the $S = {}^3/_2$ resonance precluded more detailed analysis. The addition of 55% (v/v) PEG does not affect the properties of the $S = {}^3/_2$ components of either the D14C/C17S or D14C/C56S samples.

VTMCD Spectroscopy. Figure 5 shows a comparison of the VTMCD spectra of dithionite-reduced D14C/C11S, D14S, and D14C/C56S Pf Fd in the UV−visible region. Reduced samples of the D14C/C17S variant in the presence of 55% (v/v) PEG showed VTMCD spectra indicative of partial degradation to $S = 2$ $[Fe_3S_4]^0$ clusters. These clusters have much greater (4−6 times) MCD intensity than $[Fe_4S_4]^+$ clusters at liquid He temperatures and hence dominate the VTMCD, even if present as minor components. For this reason, the VTMCD spectrum of the reduced D14C/C17S variant is not shown. Biological and synthetic $[Fe_4S_4]^+$ clusters with $S = {}^1/_2$ ground states give rise to characteristic low-temperature MCD spectra consisting of broad positive bands centered between 700−760 and 520−560 nm, multiple positive bands in the region from 350 to 550 nm, and pronounced negative features between 300−330 and 580−700 nm (*56*, *57*). The VTMCD spectra of the reduced D14C and D14C/C11S variants conform to this pattern, and the spectrum of the former is almost identical to those of reduced 8Fe and 4Fe Fds which have $[Fe_4S_4]^+$ clusters with complete cysteinyl ligation. Studies involving Pf Fd, the nitrogenase Fe protein, and synthetic clusters involving mixed spin $[Fe_4S_4]^+$ clusters have shown that the most distinguishing MCD characteristic that differentiates clusters with $S = {}^1/_2$ and $S = {}^3/_2$ ground states lies in the absence of a pronounced negative feature centered between 580 and 700 nm in $S =$

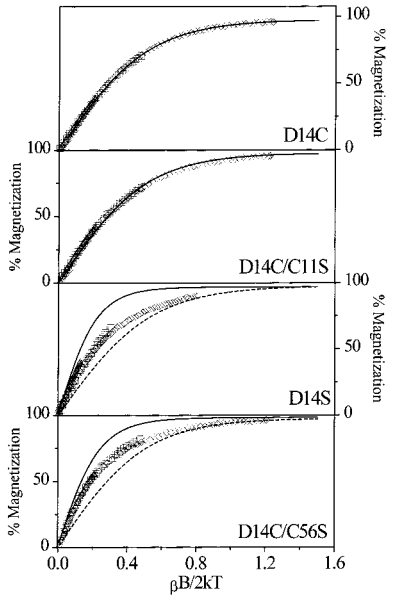

FIGURE 6: MCD magnetization data for $[Fe_4S_4]^+$ centers in dithionite-reduced D14C, D14C/C11S, D14S, and D14C/C56S Pf Fd. The samples are described in the legend of Figure 5. D14C magnetization was at 530 nm, with magnetic fields between 0 and 6.0 T at (◇) 1.63, (□) 4.22, and (△) 9.68 K. The solid line depicts the theoretical magnetization data for an $S = {}^1/_2$ ground state based on the EPR-determined g-values ($g_{||} = 2.08$, $g_\perp = 1.91$, and $m_z/m_{xy} = 1$). D14C/C11S magnetization was at 713 nm, with magnetic fields between 0 and 6.0 T at (◇) 1.65, (□) 4.22, and (△) 9.68 K. The solid line depicts the theoretical magnetization data for an $S = {}^1/_2$ ground state based on the EPR-determined g-values ($g_{||} = 2.03$, $g_\perp = 1.86$, and $m_z/m_{xy} = 1$). D14S magnetization was at 525 nm, with magnetic fields between 0 and 4.5 T at (◇) 1.61, (□) 4.22, and (△) 10.3 K. The dashed line depicts the theoretical magnetization data for an $S = {}^1/_2$ ground state based on the EPR determined g-values ($g_{||} = 2.07$, $g_\perp = 1.87$, and $m_z/m_{xy} = 1$). The solid line depicts the theoretical magnetization data for an $S = {}^3/_2$ ground state with the EPR-determined g-values ($g_{||} = 5.69$, $g_\perp = 2.52$, and $m_z/m_{xy} = 0$). D14C/C56S magnetization was at 740 nm, with magnetic fields between 0 and 6.0 T at (◇) 1.73, (□) 4.22, and (△) 9.66 K. The dashed line depicts the theoretical magnetization data for an $S = {}^1/_2$ ground state with the EPR-determined g-values ($g_{||} = 2.06$, $g_\perp = 1.87$, and $m_z/m_{xy} = 1$). The solid line depicts the theoretical magnetization data for an $S = {}^3/_2$ ground state with the EPR-determined g-values ($g_{||} = 5.28$, $g_\perp = 2.34$, and $m_z/m_{xy} = 0$). All theoretical magnetization data have been computed using the equation in ref *60*.

$^3/_2$ $[Fe_4S_4]^+$ (*2*, *57*). In accord with this, the D14C/C11S and D14C variants have more intense negative features centered at ~650 nm than both D14S and D14C/C56S which are mixed-spin systems. The VTMCD spectra for these four variants also exhibit marked differences between 250 and 400 nm, but detailed assignments are not yet available in this region for any $[Fe_4S_4]^+$ cluster. All four variants exhibit an intense positive band in the 700−800 nm region, and recent VTMCD studies of valence-delocalized $S = {}^9/_2$ $[Fe_2S_2]^+$ clusters in mutant forms of a 2Fe Fd (*58*, *59*) indicate that this feature is the hallmark of a valence-delocalized $Fe^{2.5+}Fe^{2.5+}$ pair (*59*).

The spin state assignments deduced from EPR and the VTMCD spectra have been further substantiated by MCD magnetization data (see Figure 6). MCD magnetization data for the reduced D14C and D14C/C11S variants, collected at 530 and 713 nm, respectively, are indicative of pure $S = {}^1/_2$ ground states. At all temperatures, the data are well fit by theoretical plots constructed using the EPR-determined

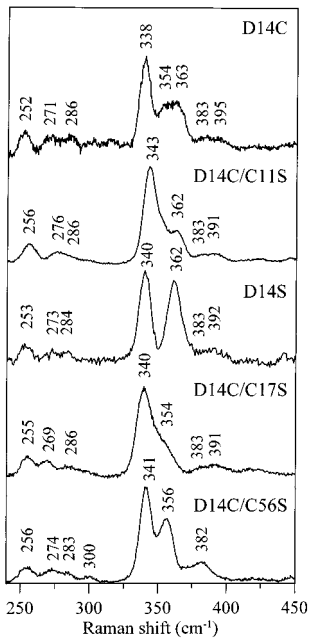

FIGURE 7: Resonance Raman spectra of $[Fe_4S_4]^{2+/+}$ centers in air-oxidized D14C, D14C/C11S, D14S, D14C/C17S, and D14C/C56S Pf Fd, obtained with 457.9 nm excitation. All spectra were recorded for samples (1−3 mM) in 100 mM Tris-HCl buffer (pH 7.8) that were frozen at 28 K. Each scan involved photon counting for 1 s every 0.5 cm^{-1}, with a spectral bandwidth of 6 cm^{-1}. For each spectrum, the vibrational modes originating from the frozen buffer solution have been subtracted after normalizing the intensities of the "ice band" at 231 cm^{-1}, and a linear ramp fluorescence baseline has also been subtracted. The conditions of measurement were as follows: D14C, 85 mW laser power at the sample and 14 scans; D14C/C11S, 89 mW laser power and 43 scans; D14S, 70 mW laser power and 25 scans; D14C/C17S, 84 mW laser power and 38 scans; and D14C/C56S, 86 mW laser power and 41 scans.

g-values for the $S = {}^1/_2$ ground state. In contrast, magnetization data for both the reduced D14S and D14C/C56S variants, collected at 525 and 740 nm, respectively, exhibit a degree of "nesting", which results from differential population and field-induced mixing of the zero-field components of an $S > {}^1/_2$ ground state. In addition, both of these variants exhibit magnetization curves at the lowest temperature that are intermediate between those expected for either a pure $S = {}^1/_2$ or $S = {}^3/_2$ ground state. Overall, the data are completely consistent with the 40:60 mixture of $S = {}^3/_2$ and $S = {}^1/_2$ ground states deduced by the EPR studies.

RR Spectroscopy. The RR spectra in the Fe−S stretching region of the $[Fe_4S_4]^{2+}$ centers in air-oxidized D14C/C11S, D14S, D14C/C17S, and D14C/C56S Pf Fd using 457.9 nm excitation are compared in Figure 7. The most complete analysis of a biological $[Fe_4S_4]^{2+}$ cluster comes from studies of the all-cysteinyl-ligated cluster in Cp 8Fe Fd. Vibrational assignments for this system were made under effective D_{2d} symmetry on the basis of ^{34}S and ^{54}Fe isotope shifts as well as extensive studies on the analogous model compound, $(Et_4N)_2[Fe_4S_4(SCH_2Ph)_4]$ (*61*). These assignments have previously been extended to wild-type Pf 4Fe Fd under effective C_{3v} symmetry (due to the aspartyl ligation at one Fe site), on the basis of the observation of parallel ^{34}S and ^{54}Fe isotope shifts (*62*) (see Table 1). In both cases, the vibrations are categorized as predominantly Fe−S^b or Fe−S^t (S^b being bridging S and S^t being terminal or cysteinyl S) on the basis of the magnitude of the $^{34}S^b$ isotope shifts. The

Table 1: Fe−S Stretching Frequencies (cm^{-1}) and Vibrational Assignments for $[Fe_4S_4]^{2+}$ Clusters in Cp Fd and Wild-Type, D14C, D14C/C11S, D14S, D14C/C17S, and D14C/C56S Pf Fd

$Fe_4S^b_4S^t_4$ D_{2d} (T_d)	Cp Fd[a]	D14C Pf Fd	$Fe_4S^b_4S^t_3$ C_{3v} (T_d)	WT Pf Fd[a]	D14C/C11S Pf Fd	D14S Pf Fd	D14C/C17 S Pf Fd	D14C/C56S Pf Fd
				Mainly Terminal $\nu(Fe-S^t)$				
A_1 (A_1)	395 (3.9)	395	A_1 (A_1)	394 (2.6)	391	392	391	382
E (T_2)	363 (2.0)	363	E (E)	363 (2.0)	362	362	354 (sh)	356
B_2 (T_2)	351 (0.7)	354						
				Mainly Bridging $\nu(Fe-S^b)$				
B_2, E (T_2)	380 (5.6)	383	A_1, E (T_2)	374 (5.0)	383	383 (sh)	383	382
A_1 (A_1)	338 (7.0)	338	A_1 (A_1)	342 (5.2)	343	340	340	341
A_1 (E)	298 (4.9)		E (E)	296 (4.6)				300
B_1 (E)/E (T_1)	276 (4.5)	286	E (T_1)	282 (4.6)	286 (sh)	284	286	283
A_2 (T_1)	266 (4.0)	271	A_2 (T_1)	269 (5.0)	276	273	269	274
B_2, E (T_2)	251 (6.2)	252	A_1, E (T_2)	253 (5.0)	256	253	255	256

[a] Numbers in parentheses are $^{34}S^b$ downshifts in cm^{-1}. Vibrational assignments and ^{34}S isotope shifts for Cp Fd and WT Pf Fd are taken from refs *61* and *62*, respectively.

RR spectra of the $[Fe_4S_4]^{2+}$ centers in wild-type Pf Fd and Cp Fd differ in two main respects, both of which can be attributed to the noncysteinyl ligation of a specific Fe atom in Pf Fd. First, only a single asymmetric Fe−S^t stretching mode is observed in Pf Fd at 363 cm^{-1} as compared to two distinct bands at 363 and 351 cm^{-1} in Cp Fd (*2*). Second, the frequency of the totally symmetric (A_1) Fe−S^b breathing mode in wild-type Pf Fd is observed at 342 cm^{-1} which is 4 cm^{-1} higher than in Cp Fd (*2*).

The RR spectra of air-oxidized D14C, D14C/C11S, D14S, D14C/C17S, and D14C/C56S Pf Fd are all indicative of $[Fe_4S_4]^{2+}$ clusters and can readily be assigned by analogy with Cp Fd or wild-type Pf Fd (see Table 1). As expected, the RR spectrum of the D14C variant closely resembles that of the all-cysteinyl-ligated clusters in Cp Fd with a split asymmetric Fe−S^t stretching mode at 354 and 363 cm^{-1} and the totally symmetric (A_1) Fe−S^b breathing mode at 338 cm^{-1}, i.e., 4 cm^{-1} lower than in wild-type Pf Fd. In contrast, the four serine variants have totally symmetric (A_1) Fe−S^b breathing modes in the range established for $[Fe_4S_4]^{2+}$ clusters with one oxygenic ligand, 340−343 cm^{-1} (*2*), and outside of the range established for biological and synthetic $[Fe_4S_4]^{2+}$ clusters with complete cysteinyl ligation, 333−339 cm^{-1} (*2*). Each of the four serine variants has a single broad band that can be assigned to the asymmetric Fe−S^t stretching mode (see Table 1). Moreover, the only major variation in the spectra of the four serine mutants lies in the frequencies and relative intensities of the symmetric and asymmetric Fe−S^t modes which lie in the ranges of 382−392 and 354−362 cm^{-1}, respectively. This most likely reflects changes in cysteinyl Fe−S_γ−C_β−C_α dihedral angles and/or changes in hydrogen bonding to cysteinyl S atoms and is consistent with a different set of three cysteines acting as ligands in each of the four serine variants. Hence, the resonance Raman results clearly support the presence of a $[Fe_4S_4]^{2+}$ cluster with one oxygenic ligand in each of the four serine variants. However, these RR results do not address the question of whether the noncysteinyl ligation is provided by serinate or water.

Electrochemistry. The midpoint potentials of the $[Fe_4S_4]^{2+,+}$ couples in D14C, D14C/C11S, D14S, D14C/C17S, and D14C/C56S Pf Fd were determined to be −427, −430, −505, −433, and −476 mV, respectively, by cyclic voltammetry at 23 °C and pH 7.0 at a glassy carbon electrode (see Table 2). These values provide a rationalization of the UV−visible absorption and EPR studies of D14S and D14C/C56S Pf Fd at pH 7.8 which demonstrated only partial reduction (∼50 and 80%, respectively) using dithionite [$E_m \sim -500$ mV at pH 8.0 (*63*)]. Plots of the pH dependence of the midpoint potentials are shown in Figure 8. The midpoint potentials of the D14C/C11S and D14C/C17S Fds are essentially invariant over the pH range of 4.0−10.0 (slopes of 0.8 and −3.9 mV/pH unit, respectively) and are similar

Table 2: Midpoint Potentials and Kinetic Parameters for D14C, D14C/C11S, D14S, D14C/C17S, and D14C/C56S Pf 4Fe Fd

Fd variant	E_m (mV vs SHE at pH 7)	POR/FNOR[a] K_m (μM)	POR/FNOR[a] V_m (units/mg)[b]
D14 (WT)[c]	−368	1.7 (0.3)	5.5 (0.3)
D14C[c]	−427	0.2 (0.05)	6.4 (0.3)
D14C/C11S	−430	0.7 (0.2)	9.1 (0.6)
D14S[c]	−505	0.5 (0.1)	6.8 (0.3)
D14C/C17S	−433	0.9 (0.2)	8.5 (0.4)
D14C/C56S	−476	1.2 (0.2)	8.7 (0.4)

[a] Kinetic parameters in the coupled POR/FNOR system measured at 80 °C and pH 8.0 as described in Materials and Methods. Standard deviations are given in parentheses. [b] One unit per milligram is the reduction of 2 μmol of Fd min^{-1} mg of $FNOR^{-1}$. [c] Taken from ref *43*.

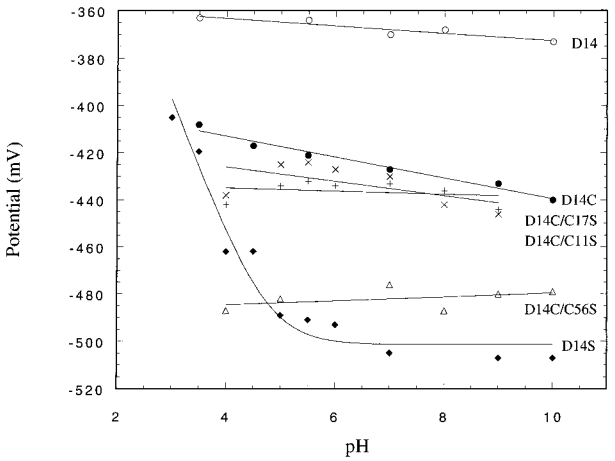

FIGURE 8: pH dependence of the midpoint potentials for the $[Fe_4S_4]^{2+,+}$ couples in wild-type and variant forms of Pf Fd: wild type (○), D14C (●), D14C/C11S (×), D14S (◆), D14C/C17S (+), and D14C/C56S (△). The values were obtained at 23 °C as described in Materials and Methods. The data for the wild type, D14C, and D14S are taken from ref *43* and are shown to facilitate comparison. All potentials are relative to the standard hydrogen electrode.

to that of the all-cysteinyl-ligated cluster in the D14C variant (*43*, *45*). The midpoint potential of the D14C/C56S variant is also essentially pH-independent over the pH range of 4.0−10.0, although the addition of a Ser ligand at this cluster-ligating position results in a 49 mV decrease in potential compared to that of D14C. D14S has the lowest potential at pH 7, with a 78 mV decrease in potential compared to that of D14C, and the midpoint potential of the D14S variant exhibits a marked pH dependence at low pH values with an increase of 55 mV/pH unit over the pH range of 3.0−5.0 (*43*, *45*). This is indicative of the uptake of one proton upon one-electron reduction, and fits to the Nernst equation indicate protonation of the reduced cluster with a pK_a of 4.75 ± 0.13 (*43*, *45*).

Biological Activity Assays. The biological activity of the double mutants of Pf Fd was determined using a coupled assay system. In this two-step assay, Fd is first reduced using an excess of POR (eq 1), and then a second enzyme, FNOR, reduces NADP using electrons from the reduced Fd (eq 2).

$$\text{pyruvate} + \text{CoASH} + 2\text{Fd}_{ox} \rightarrow \text{acetyl-CoA} + \text{CO}_2 + \text{H}^+ + 2\text{Fd}_{red} \quad (1)$$

$$2\text{Fd}_{red} + \text{H}^+ + \text{NADP} \rightarrow \text{NADPH} + 2\text{Fd}_{ox} \quad (2)$$

The overall effect of the assay is to link pyruvate oxidation to NADP reduction through POR, Fd, and FNOR. Previous work has shown that the assay assesses the interaction of Fd with FNOR (*43*) and, compared to measuring the direct reduction of Fd by POR (eq 3), negates possible problems arising from the low reduction potentials of some Fd variants. For example, an excess of POR in the assay mixture, whose redox potential at pH 8.0 and 80 °C is approximately −520 mV, will completely reduce Fd variants even with very low potentials, such as the D14S mutant (*43*). Thus, the reduction potentials of all the serine variants (Table 2) should not be a factor in the coupled assay system. The reduction potential of FNOR is approximately −250 mV at pH 8.0 and 80 °C (*43*).

As shown in Table 2, the 4Fe forms of all four serine variants were active in the coupled assay system. The data for the D14S mutant, as well as for the wild-type and D14C forms, have been previously been reported (*43*) and are included in Table 2 for comparison. The apparent K_m and V_m values for the double mutants were all in the same range as for the D14S mutant. It therefore appears that the affinity of FNOR for the Fd and the electron transfer capabilities of the Fd are not affected by the location of the serinate ligand within the coordination sphere of the cluster. Even though this assay was designed to assess the FNOR−Fd interaction, the results are consistent with POR being able to efficiently reduce each of the Fd variants. Although kinetic parameters for the interaction between the Fd variants and POR are not available from this assay, electron transfer and/or association must still be able to proceed at a significant rate for the second step of the reaction to be unaffected. These results therefore show that the mode of ligation at each Fe atom in the cluster has little effect on the interaction and the electron transfer between Fd and FNOR.

DISCUSSION

The spectroscopic and redox results presented in this work provide unambiguous evidence for the assembly of $[Fe_4S_4]^{2+,+}$ clusters with one noncysteinyl ligand in the D14C/C11S, D14S, D14C/C17S, and D14C/C56S variants of Pf Fd. This is further substantiated by the observation that a single Fe can be removed from each of these variants via ferricyanide oxidation to yield spectroscopically distinct $[Fe_3S_4]^{+,0}$ clusters (data not shown). The resulting samples have $[Fe_3S_4]^{+,0}$ clusters in four different orientations with respect to the protein structure, and the redox and spectroscopic studies of this unique set of 3Fe Fds will be the subject of a separate paper. Although it has been possible to replace individually each of the Fe-ligating cysteines with serines in rubredoxins (*17*) and in the $[Fe_2S_2]$ clusters of fumarate reductase (*18*) and 2Fe Fds (*19*−*21*), with retention of the ability to assemble the Fe center or cluster, this is the first report of a complete set of serine mutants for a $[Fe_4S_4]$ cluster. Cysteine-to-serine substitution of the four residues ligating the $[Fe_4S_4]$ cluster in *Chromatium vinosum* HiPIP resulted in only one protein in which the cluster was assembled, that with the C77S substitution (*41*). Hence, the mutant forms of Pf Fd investigated in this work offer the first opportunity to explore the physicochemical and functional consequences of changing the site of serine ligation to a $[Fe_4S_4]^{2+,+}$ cluster.

The anomalous resonance Raman, EPR, and VTMCD properties of the $[Fe_4S_4]^{2+,+}$ clusters in these serine mutants support the view of a cluster ligated by one noncysteinate ligand, but leave open the question of the nature of this ligand, i.e., serinate or solvent (OH^- or H_2O). However, in every structurally characterized Fe−S protein in which a coordinating cysteine has been replaced by a serine without loss of the Fe or Fe−S center, NMR and/or X-ray crystallographic data have provided evidence for serinate Fe ligation (*17*, *20*, *41*, *42*). Of particular importance to this work is the NMR evidence for ligation of the $[Fe_4S_4]$ cluster in the D14S variant of Pf Fd by a serinate at position 14 (*42*). The available NMR structure of D14C Pf 4Fe Fd[2] indicates that each of the Fe sites of the $[Fe_4S_4]^{2+}$ cluster is accessible to solvent, although the one ligated by the residue at position 14 is the most exposed. Hence, we favor serinate ligation at the unique Fe site in each of the three double mutants, but NMR or X-ray crystallographic studies are clearly required for definitive assessment.

Mössbauer studies of $[Fe_4S_4]^{2+,+}$ clusters have shown that their properties can be best understood in terms of pairwise Fe interactions. Hence, the $S = 0$ ground state of the oxidized state results from antiferromagnetic interaction between two valence-delocalized pairs, and the $S = {}^1/_2$ or ${}^3/_2$ ground state of the reduced state results from antiferromagnetic interaction between the valence-delocalized and all-ferrous pairs (*3*). Moreover, VTMCD studies indicate the presence of a valence-delocalized pair in the $[Fe_4S_4]^+$ clusters in all of the variants investigated in this study. Hence, to a first approximation, it is the site potential of the reducible valence-delocalized pair that determines the redox potential. Serinate ligation stabilizes the oxidized form relative to cysteinate, and accordingly, cysteine-to-serine mutations result in a substantial decrease (50−200 mV) in the site potential of the coordinated Fe or Fe pair (*17*, *18*, *41*). Such considerations lead to a logical explanation for the redox potentials

[2] P.-L. Wang, L. Calzolai, K. Bren, Q. Teng, F. E. Jenney, P. S. Brereton, J. B. Howard, M. W. W. Adams, and G. N. La Mar, *Biochemistry* (submitted for publication).

of the four serine mutants investigated in this work. Since the midpoint potentials of the $[Fe_4S_4]^{2+,+}$ clusters in the D14C/C11S and D14C/C17S variants are not significantly changed compared to that of D14C, this suggests that the cysteines at positions 11 and 17 in the D14C variant ligate the nonreducible, valence-delocalized pair. In contrast, the midpoint potentials of the $[Fe_4S_4]^{2+,+}$ clusters in the D14S and D14C/C56S variants are decreased by 40−60 mV compared to that of D14C at pH 8, suggesting that the cysteines at positions 14 and 56 ligate the reducible valence-delocalized pair. The underlying assumption in this analysis, that the mutations do not alter the pairwise Fe interactions, is supported by recent sequence specific NMR assignments of the residues ligating the $[Fe_4S_4]^+$ clusters in the D14C and D14S variants (*42*). In the parent D14C variant, NMR studies indicate that Cys11 and Cys17 ligate the valence-delocalized pair, with Cys14 and Cys56 ligating the ferrous pair. In contrast, the reduced D14S variant was found to have comparable populations of two forms: one with the valence-delocalized pair ligated by Cys11 and Cys17 and the other with the valence-delocalized pair ligated by Cys14 and Cys56. Such behavior is consistent with serinate ligation to one of the Fe atoms of the reducible pair resulting in a decrease of the redox potential such that both valence-delocalized pairs have nearly equivalent midpoint potentials. This rationalization of the redox properties is analogous to that used for interpreting the redox and EPR properties of cysteine-to-serine variants of the $[Fe_2S_2]^{2+,+}$ cluster in fumarate reductase (*18*), except that the added electron is localized over a pair of Fe atoms on reduction of $[Fe_4S_4]^{2+}$ clusters, as opposed to a single Fe in the reduction of $[Fe_2S_2]^{2+}$ clusters. However, it is of limited use for interpreting the changes in the EPR properties of the $[Fe_4S_4]^+$ clusters in these mutants, since changes in the ligation of either the valence-delocalized or ferrous pairs might be expected to perturb the ground state properties of the cluster. More detailed analysis of the complex EPR behavior will require assessment of the pairwise Fe interactions in the three double mutants via NMR studies.

The above analysis of the midpoint potentials of serine-ligated $[Fe_4S_4]^{2+/+}$ centers assumes that serine remains coordinated as serinate in both oxidation states. For D14S Pf Fd at pH 8.0, this is supported by NMR data (*42*). However, the pH dependence of the midpoint potential below pH 6 indicates that the reduced protein undergoes protonation with a pK_a^{red} of 4.75 (*43*, *45*). Since this is not observed in the D14C and wild-type samples, the serinate oxygen is clearly the obvious candidate for protonation. Whether serine remains coordinated after protonation or is replaced by water or a protein ligand remains to be established. Dithionite is unable to reduce the cluster at pH 4.0, and attempts to reduce the cluster photochemically using deazaflavin and oxalate have thus far proven unsuccessful due to the instability of the reduced cluster at this pH. While the pK_a^{red} values vary, depending on the $Fe^{3+/2+}$ character of the Fe site, the available data suggest this may be a general property of serine-coordinated Fe−S centers. For example, pH-dependent midpoint potentials have been observed in each of the cysteine-to-serine mutants of *Clostridium pasteurianum* rubredoxin with pK_a^{red} values of about 7 and 9 (*17*) and for the C56S ($pK_a^{red} = 8.7$) and C60S ($pK_a^{red} = 9.3$) mutants of *C. pasteurianum* 2Fe Fd (*59*). In the latter case, spectroscopic studies indicate that the mutations are at the reducible Fe site (*59*). The above analysis of the redox potentials permits rationalization of pK_a^{red} values of <4 for the D14C/C11S and D14C/C17S variants, since the serinate-ligated Fe atoms do not undergo a change in formal oxidation state on reduction. The absence of a pH-dependent midpoint potential for the D14C/C56S variant could result from a pK_a^{red} of <4, the serinate ligand being inaccessible to solvent, or from a mutation-induced change in the reducible pair. Medium-dependent changes in the pairwise Fe interactions are suggested by the dramatic change in the $S = {}^1/_2$ EPR signal on addition of 55% (v//v) PEG.

The redox-dependent ligand protonation that can occur with serine coordination provides an unnecessary complication for the vast majority of [Fe_4S_4] clusters that mediate electron transfer. This presumably explains why serine coordination of [Fe_4S_4] centers has yet to be encountered in any indigenous cluster. However, it could provide a mechanism for coupling proton and electron transfer provided pK_a^{red} and pK_a^{ox} are above and below the physiological pH, respectively. In other words, the serine would be protonated at physiological pH in the reduced state, and deprotonated (and ligating) in the oxidized state. Although crystallographic studies of the oxidized and reduced forms of the double-cubane nitrogenase P-clusters raised the possibility that this may be role of the serine ligand in this case (*11*), subsequent mutagenesis studies have shown that the ligating serine residue is not responsible for the observed pH dependence of the midpoint potential (*12*).

The EPR and VTMCD results for the $[Fe_4S_4]^+$ clusters in the four serine variants of Pf Fd indicate that each has a mixed-spin $S = {}^1/_2$ and ${}^3/_2$ ground state with the notable exception of D14C/C11S which is 100% $S = {}^1/_2$. In light of the room-temperature NMR results which are best interpreted in terms of $S = {}^1/_2$ ground states for the $[Fe_4S_4]^+$ clusters in the wild type, D14S, and D14C (*42*), it is possible that the $S = {}^3/_2$ components in the serine variants investigated in this work are artifacts of freezing, resulting from an undefined structural perturbation that alters the spin of the valence-delocalized or ferrous pairs. It is clear, however, that noncysteinyl ligation at a specific Fe site is necessary but not sufficient for obtaining $S = {}^3/_2$ $[Fe_4S_4]^+$ clusters at low temperatures in proteins with a Fd-like arrangement of coordinating residues. This result serves to underline the complexity of predicting and interpreting the ground state properties of biological $[Fe_4S_4]^+$ clusters. For example, homogeneous $S = {}^1/_2$ ground states are observed for the $[Fe_4S_4]^+$ cluster in D14C Pf Fd and all known examples of bacterial 4Fe and 8Fe Fds with complete cysteinyl ligation. However, there are several crystallographically characterized examples of all-cysteinyl-ligated $[Fe_4S_4]^+$ clusters, albeit with non-Fd-like arrangements of cysteines, that exhibit $S = {}^3/_2$ ground states, e.g., Pf aldehyde ferredoxin oxidoreductases (*64*), nitrogenase iron protein (*57*, *65*), and *Bacillus subtilis* amidotransferase (*66*). Conversely, although noncysteinyl ligation at a unique Fe site is responsible for $S = {}^3/_2$ $[Fe_4S_4]^+$ clusters in Fds, there are well-defined examples of $[Fe_4S4]^+$ clusters with one oxygenic ligand that are 100% $S = {}^1/_2$, e.g., aconitase (*6*) and the D14C/C11S Pf Fd studied in this work.

The ability of the $[Fe_4S_4]^{2+,+}$ cluster in Fd to participate in electron transfer between Fd and FNOR appears to be

unaffected by the ligation of any one of its Fe atoms by a serinate residue. In accord with previous studies of Pf Fd variants (*43*), this suggests that the reduction potential of a given Fd protein is the primary factor in determining its ability to function as an electron donor to FNOR. All four of the serine variants investigated in the work have reduction potentials that are low enough that the Fd to FNOR electron-transfer reaction is not limited. Therefore, no trend between V_m and redox potential was evident or expected for these variants. A recent crystallographic study has shown that the region between residues 13 and 19 in Pf Fd is the primary region involved in the interaction with formaldehyde ferredoxin oxidoreductase, another of its physiological redox partners (*67*). This further raises speculation that cluster coordination by Asp14 plays an important role in wild-type Pf Fd, in either mediating or gating electron transfer (*16*). However, no evidence of a specific role for aspartyl cluster ligation in redox reactions with POR and FNOR has emerged from these mutagenesis studies.

REFERENCES

1. Aono, S., Bryant, F. O., and Adams, M. W. W. (1989) *J. Bacteriol. 171*, 3433−3439.
2. Conover, R. C., Kowal, A. T., Fu, W., Park, J.-B., Aono, S., Adams, M. W. W., and Johnson, M. K. (1990) *J. Biol. Chem. 265*, 8533−8541.
3. Beinert, H., Holm, R. H., and Münck, E. (1997) *Science 277*, 653−659.
4. Flint, D. H., and Allen, R. M. (1996) *Chem. Rev. 96*, 2315−2334.
5. Johnson, M. K. (1998) *Curr. Opin. Chem. Biol. 2*, 173−181.
6. Beinert, H., Kennedy, M. C., and Stout, C. D. (1996) *Chem. Rev. 96*, 2335−2373.
7. Khoroshilova, N., Popescu, C., Münck, E., Beinert, H., and Kiley, P. J. (1997) *Proc. Natl. Acad. Sci. U.S.A. 94*, 6087−6092.
8. Ding, H., Hidalgo, E., and Demple, B. (1996) *J. Biol. Chem. 271*, 33173−33175.
9. Gauga, P., and Weiss, B. (1996) *Proc. Natl. Acad. Sci. U.S.A. 93*, 10094−10098.
10. Sellers, V. M., Johnson, M. K., and Dailey, H. A. (1996) *Biochemistry 35*, 2699−2704.
11. Peters, J. W., Stowell, S. M., Finnegan, M. A., Johnson, M. K., and Rees, D. C. (1997) *Biochemistry 36*, 1181−1187.
12. Lanzilotta, W. N., Christiansen, J., Dean, D. R., and Seefeldt, L. C. (1998) *Biochemistry 37*, 11376−11384.
13. Link, T. A., Hagen, W. R., Pierik, A. J., Assmann, C., and von Jagow, G. (1992) *Eur. J. Biochem. 208*, 685−691.
14. Volbeda, A., Charon, M.-H., Piras, P., Hatchikian, E. C., Frey, M., and Fontecilla-Camps, J. C. (1995) *Nature 373*, 580−587.
15. Peters, J. W., Lanzilotta, W. N., Lemon, B. J., and Seefeldt, L. C. (1998) *Science 282*, 1853−1858.
16. Calzolai, L., Zhou, Z. H., Adams, M. W. W., and La Mar, G. N. (1996) *J. Am. Chem. Soc. 118*, 2513−2514.
17. Xiao, Z., Lavery, M. L., Ayhan, M., Scrofani, S. D. B., Wilce, M. C. J., Guss, J. M., Tregloan, P. A., George, G. N., and Wedd, A. G. (1998) *J. Am. Chem. Soc. 120*, 4135−4150.
18. Werth, M. T., Cecchini, G., Manodori, A., Ackrell, B. A. C., Schröder, I., Gunsalus, R. P., and Johnson, M. K. (1990) *Proc. Natl. Acad. Sci. U.S.A. 87*, 8965−8969.
19. Cheng, H., Xia, B., Reed, G. H., and Markley, J. L. (1994) *Biochemistry 33*, 3155−3164.
20. Hurley, J. K., Weber-Main, A. M., Hodges, A. E., Stankovich, M. T., Benning, M. M., Holden, H. M., Cheng, H., Xia, B., Markley, J. L., Genzor, C., Gomez-Moreno, C., Hafezi, R., and Tollin, G. (1997) *Biochemistry 36*, 15109−15117.
21. Xia, B., Cheng, H., Bandarian, V., Reed, G. H., and Markley, J. L. (1996) *Biochemistry 35*, 9488−9495.
22. Moulis, J.-M., Davasse, V., Golinelli, M.-P., Meyer, J., and Quinkal, I. (1996) *J. Biol. Inorg. Chem. 1*, 2−14.
23. Zhao, J. D., Li, N., Warren, P. V., Golbeck, J. H., and Bryant, D. A. (1992) *Biochemistry 31*, 5093−5099.
24. Mehari, T., Qiao, F. Y., Scott, M. P., Nellis, D. F., Zhao, J. D., Bryant, D. A., and Golbeck, J. H. (1995) *J. Biol. Chem. 270*, 28108−28117.
25. Yu, L. A., Vassiliev, I. R., Jung, Y. S., Bryant, D. A., and Golbeck, J. H. (1995) *J. Biol. Chem. 270*, 28118−28125.
26. Rothery, R. A., and Weiner, J. H. (1991) *Biochemistry 30*, 8305−8310.
27. Augier, V., Guigliarelli, B., Asso, M., Bertrand, P., Frixon, C., Giordano, G., Chippaux, M., and Blasco, F. (1993) *Biochemistry 32*, 2013−2023.
28. Manodori, A., Cecchini, G., Schröder, I., Gunsalus, R. P., Werth, M. T., and Johnson, M. K. (1992) *Biochemistry 31*, 2703−2712.
29. Kowal, A. T., Werth, M. T., Manodori, A., Cecchini, G., Schröder, I., Gunsalus, R. P., and Johnson, M. K. (1995) *Biochemistry 34*, 12284−12293.
30. Busch, J. L. H., Breton, J. L., Barlett, B. M., Armstrong, F. A., James, R., and Thomson, A. J. (1997) *Biochem. J. 323*, 95−102.
31. Martin, A. E., Burgess, B. K., Stout, C. D., Cash, V. L., Dean, D. R., Jensen, G. M., and Stephens, P. J. (1990) *Proc. Natl. Acad. Sci. U.S.A. 87*, 598−602.
32. Iismaa, S. E., Vazquez, A. E., Jensen, G. H., Stephens, P. J., Butt, J. N., Armstrong, F. A., and Burgess, B. K. (1991) *J. Biol. Chem. 266*, 21563−21571.
33. Shen, B., Jollie, D. R., Diller, T. C., Stout, C. D., Stephens, P. J., and Burgess, B. K. (1995) *Proc. Natl. Acad. Sci. U.S.A. 92*, 10064−10068.
34. Blamey, J. M., and Adams, M. W. W. (1993) *Biochim. Biophys. Acta 1161*, 19−27.
35. Mukund, S., and Adams, M. W. W. (1995) *J. Biol. Chem. 270*, 8389−8392.
36. Mukund, S., and Adams, M. W. W. (1993) *J. Biol. Chem. 268*, 13592−13600.
37. Mai, X., and Adams, M. W. W. (1994) *J. Biol. Chem. 269*, 16726−16732.
38. Mai, X., and Adams, M. W. W. (1996) *J. Bacteriol. 178*, 5890−5896.
39. Heider, J., Mai, X., and Adams, M. W. W. (1996) *J. Bacteriol. 178*, 780−787.
40. Ma, K., and Adams, M. W. W. (1994) *J. Bacteriol. 176*, 6509−6517.
41. Babini, E., Bertini, I., Borsari, M., Capozzi, F., Dikiy, A., Eltis, L., and Luchinat, C. (1996) *J. Am. Chem. Soc. 118*, 75−80.
42. Calzolai, L., Gorst, C. M., Bren, K. L., Zhou, Z. H., Adams, M. W. W., and La Mar, G. N. (1997) *J. Am. Chem. Soc. 119*, 9341−9350.
43. Brereton, P. S., Verhagen, M. F. J. M., Zhou, Z. H., and Adams, M. W. W. (1998) *Biochemistry 37*, 7351−7362.
44. Busse, S. A., La Mar, G. N., Yu, L. P., Howard, J. B., Smith, E. T., Zhou, Z. H., and Adams, M. W. W. (1992) *Biochemistry 31*, 11952−11962.
45. Zhou, Z. H., and Adams, M. W. W. (1997) *Biochemistry 36*, 10892−10900.
46. Heltzel, A., Smith, E. T., Zhou, Z. H., Blamey, J. M., and Adams, M. W. W. (1994) *J. Bacteriol. 176*, 4790−4793.
47. Kunkel, T. A. (1985) *Proc. Natl. Acad. Sci. U.S.A. 82*, 488−492.
48. Schagger, H., and von Jagow, G. (1987) *Anal. Biochem. 166*, 368−379.
49. Hagen, W. R. (1989) *Eur. J. Biochem. 182*, 523−530.
50. Sery, A., Housset, D., Serre, L., Bonicel, J., Hatchikian, C., Frey, M., and Roth, M. (1994) *Biochemistry 33*, 15408−15417.
51. Bruschi, M. (1979) *Biochem. Biophys. Res. Commun. 91*, 623−628.
52. Fukuyama, K., Nagahara, Y., Tsukihara, T., and Katsube, Y. (1988) *J. Mol. Biol. 199*, 183−193.
53. Meyer, J., Moulis, J.-M., Scherrer, N., Gagnon, J., and Ulrich, J. (1983) *Biochem. J. 294*, 622−623.

54. Graves, M. C., Mullenbach, G. T., and Rabinowitz, J. C. (1985) *Proc. Natl. Acad. Sci. U.S.A. 82*, 1653−1657.
55. George, D. G., Hunt, L. T., Yeh, L.-S. L., and Barker, W. C. (1985) *J. Mol. Evol. 22*, 20−31.
56. Johnson, M. K., Robinson, A. E., and Thomson, A. J. (1981) in *Iron−Sulfur Proteins* (Spiro, T. G., Ed.) pp 367−406, Wiley-Interscience, New York.
57. Onate, Y. A., Finnegan, M. G., Hales, B. J., and Johnson, M. K. (1993) *Biochim. Biophys. Acta 1164*, 113−123.
58. Crouse, B. R., Meyer, J., and Johnson, M. K. (1995) *J. Am. Chem. Soc. 117*, 9612−9613.
59. Johnson, M. K., Duin, E. C., Crouse, B. R., Golinelli, M.-P., and Meyer, J. (1998) in *Spectroscopic Methods in Bioinorganic Chemistry* (Solomon, E. I., and Hodgson, K. O., Eds.) American Chemical Society Symposium Series, Vol. 692, pp 286−301, American Chemical Society, Washington, DC.
60. Bennett, D. E., and Johnson, M. K. (1987) *Biochim. Biophys. Acta 911*, 71−80.
61. Czernuszewicz, R. S., Macor, K. A., Johnson, M. K., Gewirth, A., and Spiro, T. G. (1987) *J. Am. Chem. Soc. 109*, 7178−7187.
62. Fu, W. (1990) M.S. Dissertation, University of Georgia, Athens, GA.
63. Mayhew, S. G. (1978) *Eur. J. Biochem. 85*, 535−547.
64. Koehler, B. P., Mukund, S., Conover, R. C., Dhawan, I. K., Roy, R., Adams, M. W. W., and Johnson, M. K. (1996) *J. Am. Chem. Soc. 118*, 12391−12405.
65. Lindahl, P. A., Day, E. P., Kent, T. A., Orme-Johnson, W. H., and Münck, E. (1985) *J. Biol. Chem. 260*, 11160−11173.
66. Onate, Y. A., Switzer, R. L., Vollmer, R. A., and Johnson, M. K. (1989) *J. Biol. Chem. 264*, 18386−18391.
67. Hu, Y., Faham, S., Roy, R., Adams, M. W. W., and Rees, D. C. (1999) *J. Mol. Biol. 286*, 899−914.

BI990671D